High-throughput approach for investigating interdiffusion in medium- and high-entropy alloys

Maik Rajkowski [a*], Adeline Durand [a**], James R. Morris [b***], Gunther Eggeler [a], Guillaume Laplanche [a]

[a] Institut für Werkstoffe, Ruhr-Universität Bochum, D-44801 Bochum, Germany
[b] AMES National laboratory, IA 50011, USA

* corresponding author for the DICTRA simulations: maik.rajkowski@rub.de
** corresponding author for the experimental part: adeline.durand@epfl.ch
*** corresponding author for the modeling part: morrisj@ameslab.gov

Abstract

Interdiffusion experiments are usually time-consuming and tedious since diffusion couples must be annealed at several temperatures for long times. The efforts required to study interdiffusion in multicomponent alloys increase dramatically as multiple diffusion couples are required to cover broad composition ranges and determine the diffusivities of individual elements in different chemical environments. To circumvent this challenge, we present a high-throughput approach applicable to single-phase and compositionally complex alloys, which are assumed to approximate ideal solid solutions. Here, a simple diffusion-multiple experiment combined with a physically based kinetic model is proposed to efficiently determine the diffusion coefficients of the constituent elements in quaternary CrFeCoNi alloys. Compared with tracer diffusivities reported in the literature, the results thus obtained do not differ by more than a factor of two and were obtained from a single interdiffusion experiment. In contrast, the diffusivities simulated with commercial mobility and thermodynamic databases are strongly overestimated by a factor ranging from 1 to 16. Therefore, our approach enables high-throughput determination of diffusivities and can help in the design of alloys for high-temperature applications where diffusion plays a key role.

Keywords: Multicomponent diffusion; High-entropy alloys (HEAs); Vacancies; Kinetics; Interdiffusion; Solid solution

1. Introduction

Diffusion is one of the most studied subjects in materials science. It governs many important phenomena determining fundamental properties of materials,[1,2] *e.g.*, microstructure evolution during high-temperature annealing,[3,4] phase transformation and particle growth,[5] creep,[6,7] and oxidation.[8,9] Since most of the structural alloys consist of a major base element (e.g., steels: Fe, light metals: Al, superalloys: Ni) whose properties are altered by small additions of other elements, it is possible to relate them to diffusion in pure metals because solvent and solutes can be clearly identified, e.g., diffusion of Cr (solute) in pure iron (solvent) for ferritic stainless steels. This approximation no longer holds in the case of medium- and high-entropy alloys (MEAs and HEAs), which have attracted considerable attention in the scientific community during the last two decades.[10-12] Since single-phase MEAs and HEAs consist of several elements in nearly equiatomic proportions, the concept of solvent and solute atoms does not apply, and new approaches must be developed to describe diffusion in these compositionally complex alloys.[13-23]

In this context, we recently proposed a new method combining experimental and modeling efforts to study interdiffusion processes in single-phase FCC CrFeCoNi MEAs, assuming that the alloys behave as ideal solid solutions.[24] From an experimental point of view, six independent pseudo-binary diffusion couples [14] were mounted in a diffusion multiple [25,26] and annealed for different times and temperatures. As all the diffusion couples were simultaneously annealed at the same temperature for the same duration, this not only considerably accelerated the study of interdiffusion but also greatly reduced the uncertainties that would arise from multiple independent experiments. As an example, one of the diffusion couples was $Cr_{29}Fe_{29}Co_{29}\boldsymbol{Ni_{13}}/\boldsymbol{Cr_{13}}Fe_{29}Co_{29}Ni_{29}$ where, for one side of the couple, the Ni-concentration was reduced to 13 at.% (emboldened and italicized for clarity) and balanced by increasing the concentrations of the three other elements to 29 at.% each. Similarly, the other side of the couple

had Cr reduced to 13 at.% and balanced by increasing the others. After diffusion annealing, the concentration profiles of the different elements can be divided into two categories: the *interdiffusing elements* with significant initial concentration gradients for which notable diffusion occurs (Cr and Ni in the previous example, e.g., Fig. 1a), and the *background elements* (Co and Fe). While the concentrations of the background elements were initially homogeneous throughout the pseudo-binary diffusion couple before annealing, small concentration gradients developed in several cases during annealing indicative of uphill diffusion (e.g., Fe and Co concentration profiles in Fig. 1a). Such behavior may either result from an imbalance in chemical potential between different elements, as originally observed by Darken [27] or from a purely kinetic effect arising from different vacancy exchange rates of the alloy elements.[24]

Although the physics of diffusion in multicomponent systems is well understood,[28] "commercial" databases are still unable to satisfactorily reproduce concentration profiles resulting from interdiffusion in single-phase MEAs and HEAs[1]. For instance, in Fig. 1, we compare the concentration profiles after annealing at 1173 K for 100 h obtained experimentally in Ref.[24] and simulated using the diffusion module DICTRA [31,32] of ThermoCalc2023a using the thermodynamic and mobility databases TCNI10 and MOBNI5, respectively. While uphill diffusion is evidenced experimentally for Co and Fe with the formation of a "hill" on the Cr-rich side and a valley on the Ni-rich side of the pseudo-binary diffusion couple (Fig. 1a), the DICTRA simulation (solid lines in Fig. 1b) predicts uphill diffusion for Co but a rather flat concentration profile for Fe with a slight "hill" on the Ni-rich side, in contrast to the experimental results. More importantly, the simulated width of the diffusion-affected region is about two times wider than that determined experimentally. However, it is unclear whether the

[1] It is however worth mentioning that attempts were made in the literature to develop "home-made" thermodynamic [29] B. Hallstedt, M. Noori, F. Kies, F. Oppermann, and C. Haase, Calphad **83,** 102644 (2023). and mobility databases [30] C. Zhang, F. Zhang, K. Jin, H. Bei, S. Chen, W. Cao, J. Zhu, and D. Lv, Journal of Phase Equilibria and Diffusion **38,** 434 (2017).

thermodynamic database, the mobility database, or a combination of the two is responsible for this large discrepancy.

To separate the thermodynamic and kinetic contributions to the interdiffusion process shown in Fig. 1a, additional DICTRA simulations were performed. First, the previously shown simulations were reproduced, assuming that the alloys are ideal solid solutions, see dashed concentration profiles in Fig. 1b. A comparison of the simulations in the ideal (dashed lines) and non-ideal (solid lines) cases in Fig. 1b reveals only small differences, suggesting that mobilities are probably responsible for the strongly overestimated width of the interdiffusion region compared to the experiment, while deviations from an ideal solid solution are secondary in this matter.

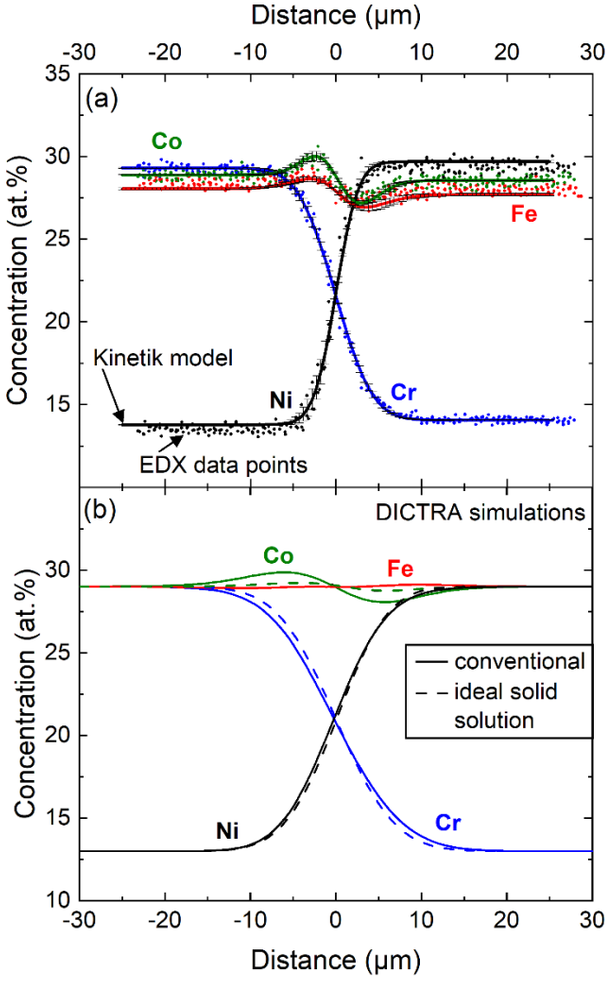

Figure 1: Concentration profiles after diffusion annealing at 1173 K for 100 h of a pseudo-binary $Cr_{29}Fe_{29}Co_{29}\boldsymbol{Ni_{13}}/\boldsymbol{Cr_{13}}Fe_{29}Co_{29}Ni_{29}$ diffusion couple from Ref. "A. Durand, L. Peng, G. Laplanche, J. R. Morris, E. P. George, and G. Eggeler, Intermetallics 122, 106789 (2020); licensed under a Creative Commons Attribution (CC-BY-NC-ND) license.". In (a), EDX data were fitted with a kinetic model (solid lines). (b) Simulations using the diffusion module DICTRA of ThermoCalc2023a in combination with the MOBNI5 and TCNI10 databases, assuming either an ideal (dashed lines) or a non-ideal solid solution. Note that the curves for Fe and Co for the ideal case in (b) overlap.

To investigate this possibility, we compare in Fig. 2 the tracer diffusivities in the equiatomic CrFeCoNi MEA determined experimentally by Vaidya et al. [33] and those calculated with DICTRA. In general, the calculated diffusivities are overestimated by a factor comprised between 1.5 and 10, showing an inappropriate description of the mobilities in the MOBNI5 database.

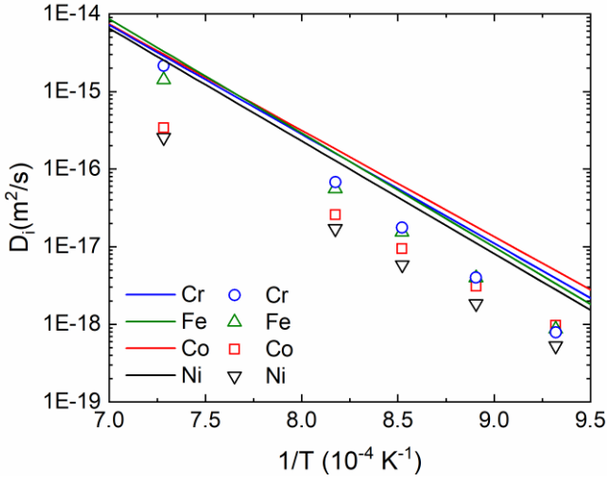

Figure 2: Comparison of tracer diffusivities D_i (i: Cr, Fe, Co, or Ni) determined experimentally (data points) by Vaidya et al. [33] and calculated using DICTRA with the MOBNI5 database (lines) in the equiatomic CrFeCoNi.

To access these data, we recently introduced a physically based, phenomenological kinetic model, which is described in Ref.[24] and summarized in section A of supplementary materials, where the alloys are assumed to behave as ideal solid solutions. Our model, based on hypotheses

previously suggested by DeHoff and Kulkarni,[34,35] couples the flux of each element with the flux of vacancies, simulating the physical process of vacancy diffusion of the different atoms. A set of only four parameters (one parameter per element describing vacancy exchange rate) is needed to simulate the simultaneous diffusion of each element in a quaternary system such as Cr-Fe-Co-Ni. From a more practical viewpoint, the experimental concentration profiles are fitted with the kinetic model by refining these four parameters from which diffusion coefficients can be deduced. The obtained results were found to be in reasonable agreement with tracer diffusion coefficients [33,36] and we could rationalize the occurrence of uphill diffusion of all the background elements. However, it is still unclear whether the obtained parameters can be extrapolated to more complex chemical environments, with both a wider range of concentrations, i.e., 15 - 35 at.% instead of 13 - 29 at.%, and a higher number of elements with significant initial concentration gradients (four in the present study compared to two in Ref.[24]). This will be addressed in the present article. Another motivation of this study is to establish the most efficient interdiffusion experiment in combination with the kinetic model allowing for the determination of the diffusion coefficients of the four constituent elements, thus enabling high-throughput characterization of interdiffusion in MEAs and HEAs.

2. Materials and experimental methods

Four alloys numbered from A to D, whose target compositions are given in the second column of Table 1, were arc melted, drop cast and homogenized following the procedure described in Ref. [24]. Note that all these quaternary alloys have two elements with low concentrations of ~15 at.% while the other two have larger contents of ~35 at.%. Metallographic specimens were cut from the homogenized alloys and polished to 1 μm followed by X-ray diffraction (XRD) and scanning electron microscope (SEM) experiments. The former were performed in a 2θ range between 20 and 120° with a 0.006°-step size using a diffractometer Philips X'Pert-MPD

PW 3040/00 equipped with a 4-bounce germanium (220) monochromator (Cu-Kα, wave length: 0.154 nm). For the microstructural and chemical investigations, a JEOL JSM-IT 300 SEM operated at 15 kV with a probe current of 60 mA was used. The compositions of the alloys were determined by energy dispersive X-ray spectroscopy (EDX) at ten separate locations (scatter: 0.5 at.%) with a live time of 60 s resulting in more than 200 000 counts, see averaged values in the third column of Table 1.

XRD in combination with SEM analyses were carried out to confirm the single-phase character of the alloys before and after diffusion annealing. A representative XRD pattern is shown in Fig. 3a where all the diffraction peaks can be indexed according to an FCC crystallographic structure. The corresponding BSE micrograph (Fig. 3b) confirms that the alloys are single phase and exhibit coarse grains (> 300 µm).

The solidus temperatures, T_s, of the alloys were determined by differential scanning calorimetry (DSC, Linseis STA PT1600). For this purpose, two tangents were drawn right before and right after the onset of the endothermic event marking the melting range on the DSC-curves upon heating and T_s was taken at the point of intersection of these tangents, e.g., Ref.[37]. Note that the T_s-values of our alloys in Table 1 do not differ from each other by more than 3%.

Four 6.5 × 6.5 × 10 mm^3 cuboidal pieces were machined from the single-phase FCC alloys *via* electric discharge machining. Their contact surfaces were ground, polished to 1 µm, plasma cleaned for 1 min in a gas mixture (25 vol.% O_2 balanced with Ar), and inserted in a sample holder made of low-carbon stainless steel, Fig. 4a. Eight screws were used to establish good contact between the alloys of the diffusion multiple. Diffusion anneals were performed in evacuated quartz tubes (3×10^{-5} mbar) at temperatures between 1173 K and 1373 K for 100 h followed by water quenching. The diffusion multiples were then cut in their middle perpendicularly to the interfaces of the diffusion couples, and metallographically prepared using the same procedure as mentioned before. It is worth mentioning that oxidation, if any, is not

expected to affect our results because our metallographic cross-sections were prepared far away from the outer surfaces of the diffusion multiple. In Fig. 4b, the colored arrows indicate the expected atomic fluxes during interdiffusion (e.g., in the diffusion couple A/B, the arrows indicate that Cr and Ni diffuse from A to B while Fe and Co move in the opposite direction).

Table 1: Targeted and experimental compositions as well as solidus temperatures of the four quaternary CrFeCoNi alloys studied in the present work. EDX, for which the absolute experimental error is ~0.5 at.%, was used for the measurements of compositions. The solidus temperatures were measured by DSC with an experimental error of ± 2 K.

Alloy	Targeted composition	Experimental composition (at.%)	Solidus Temperature, T_s (K)
A	$Cr_{35}\boldsymbol{Fe_{15}Co_{15}}Ni_{35}$	$Cr_{34.2}Fe_{15.1}Co_{15.8}Ni_{34.9}$	1668
B	$\boldsymbol{Cr_{15}}Fe_{35}Co_{35}\boldsymbol{Ni_{15}}$	$Cr_{15.9}Fe_{33.4}Co_{34.4}Ni_{16.3}$	1717
C	$\boldsymbol{Cr_{15}}Fe_{35}\boldsymbol{Co_{15}}Ni_{35}$	$Cr_{15.8}Fe_{33.7}Co_{16.0}Ni_{34.5}$	1703
D	$Cr_{35}\boldsymbol{Fe_{15}}Co_{35}\boldsymbol{Ni_{15}}$	$Cr_{34.4}Fe_{15.1}Co_{34.3}Ni_{16.2}$	1684

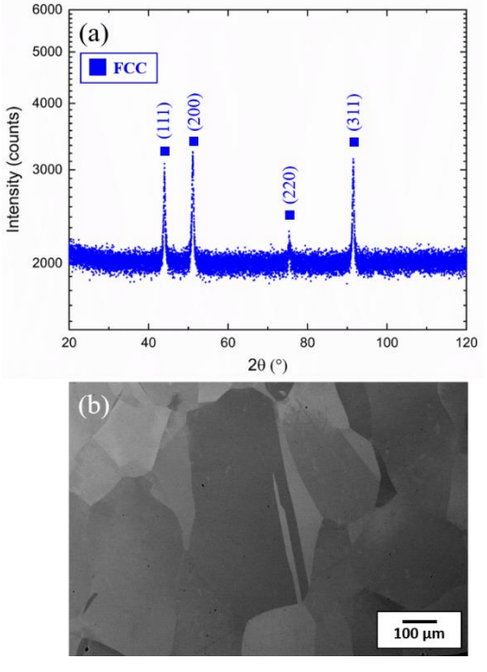

Figure 3: Phase analysis of a representative alloy after homogenization. (a) XRD pattern and (b) BSE-image showing a single-phase FCC structure.

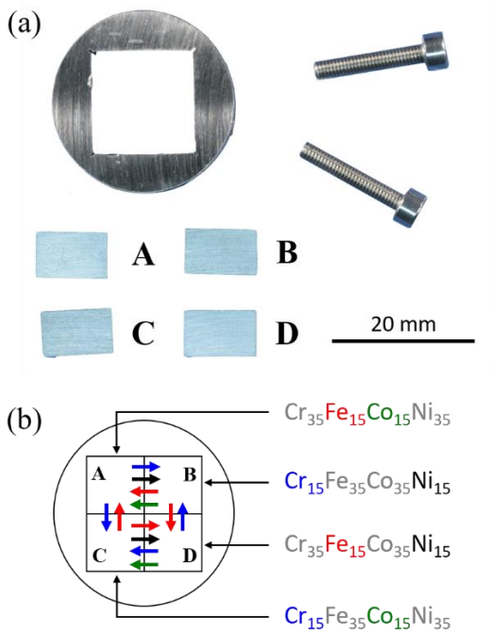

Figure 4: Diffusion multiple and interdiffusion experiments in quaternary MEAs. (a) Photograph of the stainless-steel clamping device and the tightening screws. Also shown are four cuboidal pieces before being mounted in the clamping device. (b) Schematic drawing of the diffusion-multiple experiment showing the chemical compositions of the alloys in at.% and the expected elemental diffusional fluxes (colored arrows). The diffusion multiple contains either multiple-gradients (four arrows at an interface) or pseudo-binary diffusion couples (two arrows), see text for more detail.

Our diffusion multiple contains two different diffusion couples: those with four interdiffusing elements that will be referred to as "**multiple-gradients**", e.g., A/B (Cr_{35}***$Fe_{15}Co_{15}$***Ni_{35}/***Cr_{15}***$Fe_{35}Co_{35}$***Ni_{15}***) for which the concentration profiles after a diffusion anneal at 1173 K for 100 h are shown in Fig. 5a; and "**pseudo-binaries**" with two interdiffusing elements and two "background" elements, e.g., A/C (Cr_{35}***$Fe_{15}Co_{15}$***Ni_{35}/***Cr_{15}***Fe_{35}***Co_{15}***Ni_{35}) in Fig. 5c. In total, two multiple-gradients: A/B (Cr_{35}***$Fe_{15}Co_{15}$***Ni_{35}/***Cr_{15}***$Fe_{35}Co_{35}$***Ni_{15}***) and C/D (***Cr_{15}***Fe_{35}***Co_{15}***Ni_{35}/Cr_{35}***Fe_{15}***Co_{35}***Ni_{15}***) and two pseudo-binaries (A/C and B/D), were studied. Note that no significant Kirkendall effects were identified in the investigated diffusion couples, similar to other reports in the Cr-Mn-Fe-Co-Ni system.[24,38] For more detail related to the Kirkendall effect and its determination, the reader may refer to Ref.[39,40].

After the diffusion anneals, EDX line scans (100-point analyses with 20 live seconds of recording time per point) were made across the four diffusion couples. To avoid potential artifacts, the EDX analyses were made midway between the junctions where three or four alloys are in contact and far away from grain boundaries.

3. Results and discussion

Four sets of EDX concentration profiles after annealing at 1173 K for 100 h are represented by points in Figs. 5a-d. Additional sets were also obtained for other temperatures (see Figs. S1-S6, supplementary materials). In all cases, the interdiffusing elements show the expected S-profiles and the background elements roughly retain their initially flat profiles after annealing. The fact that we do not observe significant uphill diffusion in the pseudo-binary diffusion couples A/C and B/D when Cr and Fe are the interdiffusing elements, is consistent with the results reported in Ref.[24]. Indeed, if the two interdiffusing elements have similar tracer diffusivities (as is the case for Cr and Fe in the Cr-Fe-Co-Ni system), no or negligible uphill diffusion of the background elements will be observed. In other words, the smaller the difference between the diffusivities of the diffusing elements, the weaker the uphill diffusion.

To investigate whether the concentration profiles of Fig. 5 can be predicted from our previous research focusing on CrFeCoNi alloys with different numbers of interdiffusing elements and composition ranges, the diffusivities of Cr, Fe, Co, and Ni reported in Ref.[24] and provided in the first row of data (without headers) in Table 2, were used as inputs for the kinetic model. The corresponding predictions are shown as solid lines in Fig. 5. Despite some deviations between the experimental and predicted concentration profiles, which are expected since our approach neglects non-ideal effects, our predictions are much closer to the experimental results than those obtained using DICTRA (accounting for non-ideal effects but relying on mobility databases), which overestimates the width of the diffusion region by a factor of 1 to 4 depending

on the temperature and interdiffusing elements (resulting in diffusivities that are overestimated by a factor ranging from 1 to 16), see Fig. S7-S11. This shows that if small deviations can be tolerated, the diffusivities determined from six specific pseudo-binary diffusion couples of the type $\boldsymbol{Cr_{13}}Fe_{29}Co_{29}Ni_{29}/Cr_{29}Fe_{29}Co_{29}\boldsymbol{Ni_{13}}$ [24] can be used to predict the concentration profiles in different alloys of the Cr-Fe-Co-Ni system (e.g., $\boldsymbol{Cr_{15}}Fe_{35}\boldsymbol{Co_{15}}Ni_{35}/Cr_{35}\boldsymbol{Fe_{15}}Co_{35}\boldsymbol{Ni_{15}}$) with a reasonable accuracy for such chemically complex alloys (within a factor of two for the diffusivities).

If we now compare the model diffusivities determined at 1173 K with the tracer diffusion coefficients reported for the equiatomic $Cr_{25}Fe_{25}Co_{25}Ni_{25}$ alloy by Vaidya et al.,[33,36] see last row of Table 2, it can be seen that the diffusivities do not differ by more than a factor two, which, in view of the assumptions that were made, represents a reasonable agreement for diffusion data. This arises from the fact that the following conditions are approximately fulfilled for CrFeCoNi MEAs: (1) there is no significant Kirkendall effect, (2) the alloys have similar solidus temperatures, and (3) the tracer diffusivities weakly depend on composition as shown in Ref.[30].

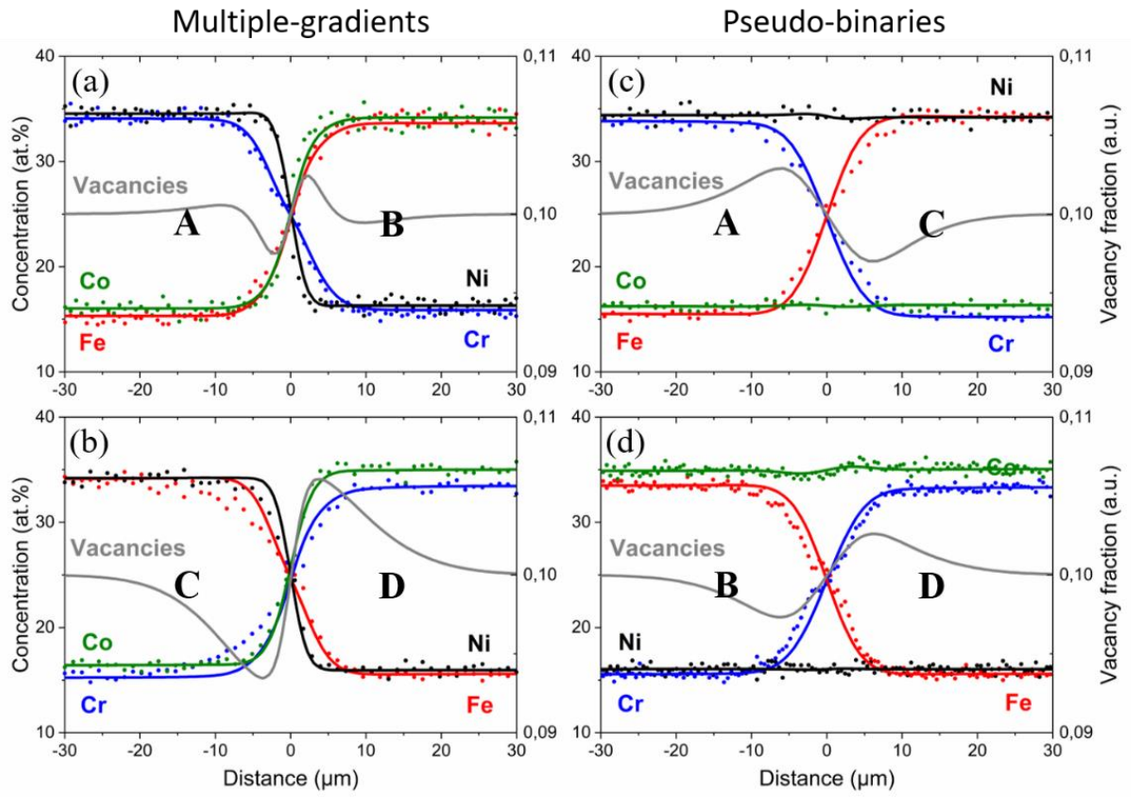

Figure 5: Concentration profiles after annealing at 1173 K for 100 h from the two multiple-gradients and two pseudo-binary diffusion couples. Points represent EDX data while colored lines are predictions obtained from our kinetic model. Diffusion couples: Multiple-gradients (a) A/B and (b) C/D, pseudo-binaries (c) A/C and (c) B/D. The kinetic-model parameters obtained in Ref.[24] from six different pseudo-binary diffusion couples (listed in Table 2) were used as inputs to predict the concentration profiles of the elements as well as the profile (gray line) of the vacancy fraction. It is worth recalling here that there is no fitting procedure involved.

It can be argued that better agreement could be obtained in Fig. 5 if non-ideal effects, as evidenced in the Cr-Fe-Co-Ni system,[16,20] were taken into account in our analysis, but if these discrepancies can be tolerated, then the diffusivities determined with our kinetic model are then equivalent to tracer diffusion coefficients, which significantly reduces the complexity of diffusion processes in CrFeCoNi alloys. In fact, the evolution of the concentration profiles can be entirely predicted with only one parameter per element, assuming that the alloys behave as ideal solid solutions.[24]

Having established the framework of diffusion processes in CrFeCoNi alloys, the following question arises: *What is the most efficient diffusion-multiple experiment, i.e., involving the least number of CrFeCoNi alloys and diffusion couples, which, in combination with our kinetic model, enables to determine the tracer diffusivities of the constituent elements?* To address this question, we now consider three distinct experimental data sets as inputs for the kinetic model:

1. Six pseudo-binaries from Ref.[24] (6 PBs)
2. Two multiple-gradients (2 MGs, A/B and C/D)
3. One multiple-gradient (1 MG, A/B).

We also introduce the parameter n representing how many times each element in each dataset has a significant initial concentration gradient in the different diffusion couples. At a given temperature, all the concentration profiles for a given data set (24 for the first, 8 for the second, and 4 for the third) were simultaneously fitted using the kinetic model to refine the diffusivities of the constituent elements. For each dataset, good fits were obtained, and the refined diffusivities are given in Table 2. For the first dataset (n = 3), the 24 experimental concentration profiles and the corresponding fits can be found in Fig. 6 of Ref.[24]. When the eight concentration profiles of the second dataset (n = 2, two MGs in Figs. 5a,b) are used to refine the model's parameters, the obtained fits in Figs. S2a,b are better than those in Fig. 5 but the

diffusivities are not significantly different from those reported in Ref.,[24] compare the first and second rows of Table 2. Besides, even though the two PBs shown in Figs. S2c,d were not used to refine the elemental diffusivities, their concentration profiles can be satisfactorily reproduced using the kinetic model. Finally, similar results are also obtained for the third data set including only one MG (n = 1, A/B, Fig. S3), and the fitted diffusivities in Table 2 do not deviate from the tracer diffusivities by more than a factor of two, i.e., the ratios of the diffusivities are smaller than two (e.g., 3.39/1.73 = 1.96 for Cr or 2.51/1.54 = 1.63, etc.).

Table 2: Comparison of the elemental diffusivities at 1173 K obtained using the kinetic model with experimental concentration profiles for either six pseudo-binary (PBs) CrFeCoNi diffusion couples of type $\boldsymbol{Cr_{13}}Fe_{29}Co_{29}Ni_{29}/Cr_{29}Fe_{29}Co_{29}\boldsymbol{Ni_{13}}$,[24] two or one multiple-gradients (MGs) diffusion couples (e.g. $\boldsymbol{Cr_{15}}Fe_{35}\boldsymbol{Co_{15}}Ni_{35}/Cr_{35}\boldsymbol{Fe_{15}}Co_{35}\boldsymbol{Ni_{15}}$, this study). Also provided are the parameter n and the tracer diffusivities reported by Vaidya et al.[33,36] for $Cr_{25}Fe_{25}Co_{25}Ni_{25}$.

Reference	Experiments	n	Elemental diffusion coefficients ($\times 10^{17}$ m^2 × s^{-1})			
-	-	-	**Cr**	**Fe**	**Co**	**Ni**
[24]	6 PBs	3	2.64	1.54	0.69	0.42
This study	2 MGs	2	3.34	2.83	0.74	0.48
This study	1 MG (A/B)	1	3.39	2.51	0.81	0.45
[33,36]	Tracer diffusion	-	1.73	1.57	0.94	0.59

The concentration profiles of either one or two MGs obtained at higher temperatures were also fitted with the kinetic model to determine the elemental diffusivities, D, of the constituent elements in CrFeCoNi alloys. The obtained results are shown as empty (2 MGs) and filled squares (1 MG) in the Arrhenius plots of Fig. 6. Also shown in Fig. 6 for comparison are the diffusivities that were reported in Ref.[24] using six pseudo-binary diffusion couples with different compositions (stars) as well as the tracer diffusion data (lines) of Vaidya et al.[33,36] determined for the equiatomic CrFeCoNi alloy. The overall reasonable agreement between all these data sets, despite the difference in investigated concentration ranges, number of

interdiffusing elements, and methods used (interdiffusion *vs.* tracer), suggests that our *D*-values do not strongly depends on composition in the studied ranges (13-35 at.% and 1153-1373 K) in agreement with the conclusions of Zhang et al.[30]. From all the data in Fig. 6, linear fits allowed to determine the pre-exponential factors, D_0, and activation enthalpies, Q, see Table 3.

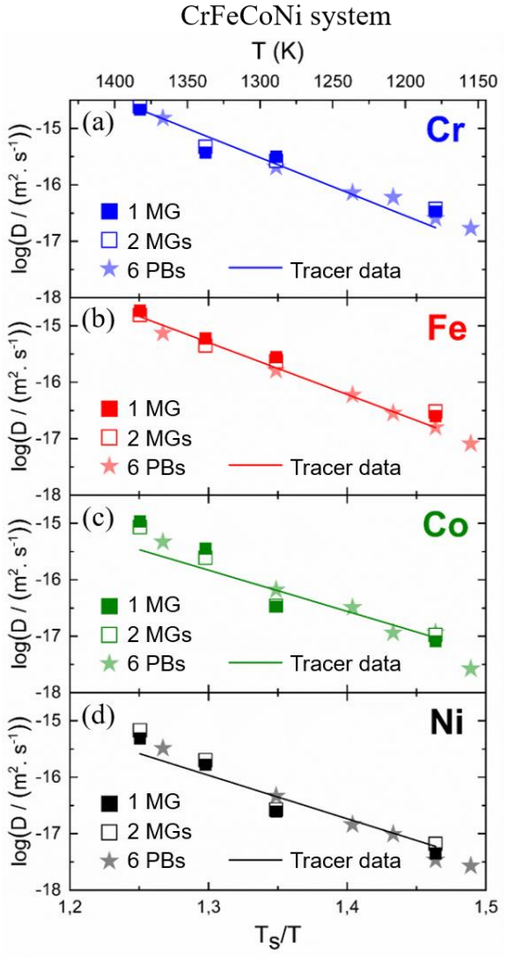

Figure 6: Arrhenius curves of diffusivities ($log\ D$) plotted against the inverse homologous temperature T_s/T for (a) Cr, (b) Fe, (c) Co, and (d) Ni in CrFeCoNi alloys. Here, T_s is the average solidus temperature of the considered diffusion couple(s). The data obtained in the present study by applying the kinetic model to our experimental data using either one (A/B) or two MGs (A/B and C/D) are shown as full and empty squares, respectively. For comparison, the data reported in Ref.[24] and obtained in different composition ranges using only pseudo-binary diffusion couples are shown as filled stars. Tracer diffusivities from Vaidya et al.[33,36] are shown as well as straight lines.

Table 3: Pre-exponential factors, D_0, and activation enthalpies, Q, calculated from the temperature dependence of the elemental diffusivities assuming that $D = D_0\ exp(-Q/(RT))$. These parameters were obtained for the Cr-Fe-Co-Ni system in the 13-35 at.% concentration and 1153-1373 K temperature ranges.[24,33,36]

Interdiffusing element	D_0 ($\times 10^4$ m^2 $\times$ s^{-1})	Q (kJ $\times$ mol^{-1})
Cr	0.68	278
Fe	0.97	285
Co	0.20	279
Ni	1.51	303

4. Conclusion

To conclude, our new approach yields similar tracer diffusivities as those reported in Refs. [24,33] but requires only one significant initial concentration gradient per element (n = 1), allowing a considerably sped up determination of the diffusivities. In other words, it is sufficient to study one diffusion couple (1 MG) with two alloys while six PBs with four alloys were previously necessary [24]. An additional advantage of our approach is that the geometry of the diffusion multiple is much simpler, which increases the probability of successful experiments, i.e., the higher the number of interfaces in the diffusion multiple, the higher the risk that some interfaces will not have a sufficient contact.

Our predictions of concentration profiles were found to be in much better agreement with experimental data than simulations of interdiffusion using commercial databases. However, it should be noted that an even higher level of accuracy could be achieved if non-ideal effects were taken into account.

Our results indicate that the diffusivities of the constituent elements of the Cr-Fe-Co-Ni system are only weakly dependent on the chemical environment in the concentration ranges studied (13-35 at.%), and the parameters determined by the kinetic model for a specific combination of diffusion couples can be used to predict the evolution of concentrations in different

concentration ranges. Our procedure may be extended to alloys consisting of more elements, provided that these alloys can be considered as ideal solid solutions that have similar solidus temperatures.

Supplementary material section

The supplementary material can be found in the online version of the article.

Acknowledgments

AD acknowledges funding by the International Max Planck Research School SurMat. GL acknowledges funding from the German Research Foundation (Deutsche Forschungsgemeinschaft DFG) through project B8 of the SFB/TR 103. MR and GL would like to thank Lars Höglund and Henrik Larsson for their help with the DICTRA simulations. The Center for interface-dominated high-performance materials (Zentrum für Grenzflächendominierte Höchstleistungswerkstoffe, ZGH) is acknowledged for the use of the Linseis STA PT1600 DSC. JRM acknowledges support by the U.S. Department of Energy, Office of Science, Basic Energy Sciences, Materials Sciences and Engineering Division.

Author declarations section

Conflict of interest: The authors have no conflicts to disclose.

Author contributions: **Maik Rajkowski:** Formal analysis (lead); Investigation (equal); Methodology (equal); Software (lead); Validation (supporting); Visualization (equal); review and editing (supporting). **Adeline Durand**: Data curation (equal); Formal analysis (equal); Investigation (equal); Methodology (lead); Validation (supporting); Visualization (supporting); writing – review and editing (supporting). **James Morris**: Software (lead); Supervision

(supporting); Writing – review and editing (equal). **Gunther Eggeler:** Conceptualization (supporting); Formal analysis (supporting); Funding acquisition (lead); Resources (lead); Writing – review and editing (supporting). **Guillaume Laplanche**: Conceptualization (lead); Data curation (supporting); Supervision (lead); Vizualization (lead); writing – original draft (lead); Writing – review and editing (lead).

Data availability statement

The data that support the findings of this study are openly available in Mendeley data repository at doi:10.17632/52gchtffvp.1

References

1 H. Mehrer, *Diffusion in solids: fundamentals, methods, materials, diffusion-controlled processes*, Vol. 155 (Springer Science & Business Media, 2007).
2 A. Paul, T. Laurila, V. Vuorinen, and S. V. Divinski, *Thermodynamics, diffusion and the Kirkendall effect in solids*, first ed. (Springer Cham, 2014).
3 Z. Wu, H. Bei, F. Otto, G. M. Pharr, and E. P. George, Intermetallics **46,** 131 (2014).
4 T. Rieger, J.-M. Joubert, R. Poulain, X. Sauvage, E. Paccou, L. Perrière, I. Guillot, G. Dirras, G. Laplanche, M. Laurent-Brocq, and J.-P. Couzinié, Journal of Alloys and Compounds **967,** 171711 (2023).
5 G. Laplanche, Acta Materialia **199,** 193 (2020).
6 D. Xie, R. Feng, P. K. Liaw, H. Bei, and Y. Gao, Intermetallics **121,** 106775 (2020).
7 U. Glatzel, F. Schleifer, C. Gadelmeier, F. Krieg, M. Müller, M. Mosbacher, and R. Völkl, Metals **11,** 1130 (2021).
8 G. Laplanche, U. F. Volkert, G. Eggeler, and E. P. George, Oxidation of Metals **85,** 629 (2016).
9 C. Stephan-Scherb, W. Schulz, M. Schneider, S. Karafiludis, and G. Laplanche, Oxidation of Metals **95,** 105 (2021).
10 M.-H. Tsai and J.-W. Yeh, Materials Research Letters **2,** 107 (2014).
11 D. Miracle and O. Senkov, Acta Materialia **122,** 448 (2017).
12 E. P. George, W. A. Curtin, and C. C. Tasan, Acta Materialia **188,** 435 (2020).
13 M. A. Dayananda and Y. H. Sohn, Metallurgical and Materials Transactions A **30,** 535 (1999).
14 K. Y. Tsai, M. H. Tsai, and J. W. Yeh, Acta Materialia **61,** 4887 (2013).
15 I. V. Belova, Y. H. Sohn, and G. E. Murch, Philosophical Magazine Letters **95,** 416 (2015).

16 V. Verma, A. Tripathi, and K. N. Kulkarni, Journal of Phase Equilibria and Diffusion **38,** 445 (2017).
17 W. Kucza, J. Dąbrowa, G. Cieślak, K. Berent, T. Kulik, and M. Danielewski, Journal of Alloys and Compounds **731,** 920 (2018).
18 K. Jin, C. Zhang, F. Zhang, and H. Bei, Materials Research Letters **6,** 293 (2018).
19 D. Gaertner, K. Abrahams, J. Kottke, V. A. Esin, I. Steinbach, G. Wilde, and S. V. Divinski, Acta Materialia **166,** 357 (2019).
20 N. Esakkiraja, A. Dash, A. Mondal, K. C. H. Kumar, and A. Paul, Materialia **16,** 101046 (2021).
21 A. Mehta, I. V. Belova, G. E. Murch, and Y. Sohn, Journal of Phase Equilibria and Diffusion **42,** 696 (2021).
22 A. Hilhorst and P. J. Jacques, Journal of Phase Equilibria and Diffusion **42,** 708 (2021).
23 J. R. Morris, in *Dynamic Processes in Solids*, edited by J. E. House (Elsevier, 2023), p. 115.
24 A. Durand, L. Peng, G. Laplanche, J. R. Morris, E. P. George, and G. Eggeler, Intermetallics **122,** 106789 (2020).
25 J.-C. Zhao, Annual Review of Materials Research **35,** 51 (2005).
26 S. Cao and J.-C. Zhao, Acta Materialia **88,** 196 (2015).
27 L. S. Darken, Trans. AIME. **180,** 430 (1949).
28 L. Zhou, M. A. Dayananda, and Y. H. Sohn, in *Handbook of Solid State Diffusion, Volume 1*, edited by A. Paul and S. Divinski (Elsevier, 2017), p. 203.
29 B. Hallstedt, M. Noori, F. Kies, F. Oppermann, and C. Haase, Calphad **83,** 102644 (2023).
30 C. Zhang, F. Zhang, K. Jin, H. Bei, S. Chen, W. Cao, J. Zhu, and D. Lv, Journal of Phase Equilibria and Diffusion **38,** 434 (2017).
31 J.-O. Andersson, T. Helander, L. Höglund, P. Shi, and B. Sundman, Calphad **26,** 273 (2002).
32 A. Borgenstam, L. Höglund, J. Ågren, and A. Engström, Journal of Phase Equilibria **21,** 269 (2000).
33 M. Vaidya, K. G. Pradeep, B. S. Murty, G. Wilde, and S. V. Divinski, Acta Materialia **146,** 211 (2018).
34 J. E. Lane and J. S. Kirkaldy, Canadian Journal of Physics **42,** 1643 (1964).
35 N. S. Kulkarni, C. V. Iswaran, and R. T. DeHoff, Acta Materialia **53,** 4097 (2005).
36 M. Vaidya, S. Trubel, B. S. Murty, G. Wilde, and S. V. Divinski, Journal of Alloys and Compounds **688,** 994 (2016).
37 C. Wagner, A. Ferrari, J. Schreuer, J.-P. Couzinié, Y. Ikeda, F. Körmann, G. Eggeler, E. P. George, and G. Laplanche, Acta Materialia **227,** 117693 (2022).
38 C.-H. Xia, J. Kundin, I. Steinbach, and S. Divinski, Acta Materialia **232,** 117966 (2022).
39 A. Paul, Thesis, 2004.
40 E. Schulz, A. Mehta, S. H. Park, and Y. Sohn, Journal of Phase Equilibria and Diffusion **40,** 156 (2019).